Published in final edited form as:
J Phys Chem B. 2010 July 22; 114(28): 9313–9321. doi:10.1021/jp104450m.

Fluorene-Based Metal-Ion Sensing Probe with High Sensitivity to Zn^{2+} and Efficient Two-photon Absorption

Kevin D. Belfield[1,2], **Mykhailo V. Bondar**[3], **Andrew Frazer**[1], **Alma R. Morales**[1], **Oleksiy D. Kachkovsky**[4], **Ivan A. Mikhailov**[5], **Artëm E. Masunov**[1,5,6], and **Olga V. Przhonska**[3]

[1] Department of Chemistry, University of Central Florida, P.O. Box 162366, Orlando, FL 32816-2366, USA

[2] CREOL, College of Optics and Photonics, University of Central Florida, P.O. Box 162366, Orlando, FL 32816-2366, USA

[3] Institute of Physics, Prospect Nauki, 46, Kiev-28, 03028, Ukraine

[4] Insitute of Organic Chemistry, Murmanskaya Street, 5, Kiev, 03094, Ukraine

[5] NanoScience Technology Center, 12424 Research Parkway, Ste 400, University of Central Florida, Orlando, FL 32826, USA

[6] Department of Physics, University of Central Florida, Orlando, FL 32816, USA

Abstract

The photophysical, photochemical, two-photon absorption (2PA), and metal ion sensing properties of a new fluorene derivative (E)-1-(7-(4-(benzo[d]thiazol-2-yl)styryl)-9,9-bis(2-(2-ethoxyethoxy)ethyl)-9H-fluoren-2-yl)-3-(2-(9,10,16,17,18,19,21,22,23,24-decahydro-6H dibenzo[h,s][1,4,7,11,14,17]trioxatriazacycloicosin-20(7H)-yl)ethyl)thiourea (**1**) were investigated in organic and aqueous media. High sensitivity and selectivity of **1** to Zn^{2+} in THF and a water/ACN mixture were shown by both absorption and fluorescence titration. The observed complexation processes corresponded to 1:1 stoichiometry with the range of binding constants ~ $(2–3)\cdot10^5$ M^{-1}. The degenerate 2PA spectra of **1** and **1**:Zn^{2+} complex were obtained in the 640–900 nm spectral range, with the maximum values of two-photon action cross section for ligand:metal complex ~ (90–130) GM, using a standard two-photon induced fluorescence methodology under femtosecond excitation. The nature of the 2PA bands was analyzed by quantum chemical methods and a specific dependence on metal ion binding processes was shown. Ratiometric fluorescence detection (420/650 nm) provided a good dynamic range (10^{-4} to 10^{-6} M) for detecting Zn^{2+}, which, along with the good photostability and 2PA properties of probe **1**. makes it a good candidate in two-photon fluorescence microscopy imaging and sensing of Zn ions.

1. Introduction

Two-photon absorbing (2PA) organic molecules with specific chemical affinity and linear photophysical properties have found utility in two-photon fluorescence microscopy (2PFM) as chemosensors for detecting metal ions in different organic and aqueous media.[1–4] Well-known advantages of 2PA processes, such as a higher excitation selectivity, deeper penetration, and photochemical stability of chemosensors under IR irradiation,[5–7] facilitate measurements of metal ion concentrations and their volumetric distribution in the medium.[8–10] To date, these investigations are of great interest for biophysical and biomedical applications,[4, 11–14] along with the development of new environmental sensing 2PA

Correspondence to: Kevin D. Belfield.

materials.[7, 9, 15] The investigations of 2PA compounds for metal ion sensing are quite limited however,[2, 5] in contrast to a large variety of organic chromophores that are known to be effective one-photon sensors.[16–19] The latter have been employed for 2PFM, though they are not optimized for two-photon excitation and result in less than satisfactory 2PA sensitivity.

The combination of efficient molecular nonlinear absorption properties with a high selectivity to metal ions is a challenging task in the development of new types of 2PA chemosensors. As an example, two aminostilbene derivatives were developed from the well-known one-photon sensor for Ca^{2+}, 1,2-bis(o-aminophenoxy)ethane-N,N,N′,N′-tetraacetic acid (BAPTA),[20, 21] with increased 2PA cross sections due to introduction of a 1,2-diphenylethene-based structural unit.[2] High Ca^{2+} affinity together with efficient two-photon action cross sections $\delta_{2PA} \cdot \Phi$ ~100 GM (δ_{2PA} and Φ are the 2PA cross section and fluorescence quantum yield, respectively) make such probes suitable in quantitative determination of Ca^{2+} in biological samples. New 2PA sensors for Pb^{2+} and Cd^{2+} based on phenylethynyl phosphine oxide derivatives with several fluorescent arms were recently reported.[5] These compounds are of interest as the first efficient 2PA sensors for Cd^{2+} and possess potential for the detection of toxic heavy metals in the environment. The effects of Mg^{2+} binding on linear spectroscopic and 2PA properties of mono- and bis-(aza-15-crown-5-ether) substituted molecules were described and the possibility of their efficient practical use in 2PFM was shown.[9]

Among other metal ions, Zn^{2+} plays a vital role in the numerous physiological processes,[16, 22] and the development of new 2PA organic molecules for selective detection of Zn^{2+} is extremely important for the investigation of biological systems by 2PFM methods. High selectivity and sensitivity for Zn^{2+} were reported for a novel 7-substituted, quinoline-based fluorescent probe (7-MOQ) in aqueous solution by the two-photon induced fluorescence method.[1] The observed fluorescence enhancement was explained by blocking the photoinduced electron transfer pathway[23] in 7-MOQ due to binding with Zn^{2+}. A branched chromophore, tris[p-(4-pyridylethynyl)phenyl]amine with pyridine terminal groups, was investigated for its ability to sense a small amount of zinc ions via a two-photon induced fluorescence enhancement mechanism.[24] Increase in the acceptor strength and a large change in dipole moment were suggested to contribute to the enhancement of the 2PA cross section upon Zn^{2+} addition. Other types of 2PA organic compounds with specific mechanisms of zinc ions sensing have also been reported.[7, 8, 25, 26]

In this paper, a new fluorene derivative, (E)-1-(7-(4-(benzo[d]thiazol-2-yl)styryl)-9,9-bis(2-(2-ethoxyethoxy)ethyl)-9H-fluoren-2-yl)-3-(2-(9,10,16,17,18,19,21,22,23,24-decahydro-6H dibenzo[h,s][1,4,7,11,14,17]trioxatriazacycloicosin-20(7H)-yl)ethyl)thiourea (**1**), that exhibited high selectivity to Zn^{2+} and efficient 2PA properties was investigated. The ligand architecture is based on a macrocycle receptor that has shown preferential binding to zinc,[27] connected to a fluorene backbone via a thiourea moiety. An analytical description of the complexation processes and quantum chemical calculations of the changes in the electronic parameters of **1** upon metal ion binding were performed. A comprehensive analysis of the linear absorption, fluorescence, and lifetime properties of **1** and its complexes with Zn^{2+} in organic solvents and aqueous medium are presented along with photochemical stability measurements. The 2PA spectra of **1** were obtained by the two-photon induced fluorescence (2PF) method[28] using 1 kHz femtosecond excitation. The effects of metal ion binding on 2PA efficiency of **1**, sensitive ratiometric Zn ion sensing parameters, and its potential applications in 2PFM are presented.

2. Experimental Section

2.1 Materials and Synthetic Procedures

1,7-Bis(2-formylphenyl)-1,4,7-trioxaheptane (**A**), oxaaza macrocycle ligand (**B**), and 2-(4-(2-(9,9-bis(2-(2-ethoxyethoxy)ethyl)-2-isothiocyanato-fluoren-7-yl)vinyl)phenyl)benzothiazole (**C**) were prepared as described previously.[27, 29, 30] All reagents and solvents were used as received from commercial suppliers unless otherwise noted. ^{1}H and ^{13}C NMR spectroscopic measurements were performed using a Varian 500 NMR spectrometer at 500 or 125 MHz, respectively, with tetramethysilane (TMS) as internal reference; ^{1}H (referenced to TMS at $\delta = 0.0$ ppm) and ^{13}C (referenced to $CDCl_3$ at $\delta = 77.0$ ppm). Chemical shifts of ^{1}H and ^{13}C spectra were interpreted with the support of CS ChemDraw Ultra version 5.0. High-resolution mass spectrometry (HR-MS) analysis was performed in the Department of Chemistry, University of Florida, Gainesville, FL.

Synthesis of (E)-1-(7-(4-(benzo[d]thiazol-2-yl)styryl)-9,9-bis(2-(2-ethoxyethoxy)ethyl)-9H-fluoren-2-yl)-3-(2-(9,10,16,17,18,19,21,22,23,24-decahydro-6H-dibenzo[h,s][1,4,7,11,14,17]trioxatriazacycloicosin-20(7H)-yl)ethyl)thiourea (1)—Oxaaza macrocycle ligand **B** (0.13 g, 0.31 mmol) was dissolved in anhydrous DMF (3 mL) under N_2, followed by slow addition of fluorene isothiocyanate **C** (0.18 g, 0.26 mmol). The clear solution was stirred at room temperature, gradually changing to a fluorescent yellow color. After 14 h, the starting material was completely consumed as determined by TLC (silica gel, EtOAc/MeOH 9:1). DMF was removed by vacuum distillation, yielding brown oil. This was then diluted with four volumes of ether to precipitate the product. The solid was collected by filtration, redissolved in a minimum volume of DMSO, and then reprecipitated by addition of ether. The solid was collected and dried to afford 0.25 g of yellow solid (85% yield, m. p. 93–94 °C). ^{1}H NMR (500 MHz, $CDCl_3$) δ/ppm 8.08, (q, J= 8.5, 3H), 7.92 (d, J= 7.5, 1H), 7.68–7.23 (m, 20H), 4.23 (bs, 6H), 3.90 (bs, 4H), 3.41 (m, 16H), 3.02 (m, 10H), 2.42 (s, 8H), and 1.25 (t, J= 6.5 Hz, 6H). ^{13}C NMR (125 MHz, $CDCl_3$): δ/ppm 180.7, 167.8, 157.2, 154.3, 149.7, 149.4, 140.4, 140.3, 135.8, 135.1, 132.5, 128.0, 127.9, 127.1, 126.9, 126.6, 126.3, 125.4, 125.0, 123.2, 123.1, 121.7, 121.1, 120.9, 120.1, 119.8, 112.2, 70.2, 69.7, 69.5, 67.2, 66.6, 66.5, 51.1, 41.2, 39.7, 15.2, 15.1. HR-MS-ESI theoretical m/z $[M+H]^+$ = 1119.54 and $[M+Na]^+$ = 1141.52, found $[M+H]^+$ = 1119.54 and $[M+Na]^+$ = 1141.52.

2.2. Linear photophysical and photochemical measurements

The molecular structure of the new fluorene-based macrocyclic chemosensor **1** is illustrated in Figure 1. All linear photophysical parameters were measured in spectroscopic grade toluene, tetrahydrofuran (THF), dichloromethane (DCM), dimethylsulfoxide (DMSO), acetonitrile (ACN), methanol (MeOH), and in an aqueous mixture of water/ACN (1:1). One-photon electronic absorption (1PA) spectra of **1** were determined with an Agilent 8453 UV–visible spectrophotometer for molecular concentrations 10^{-3} M ≤ C ≤ 10^{-6} M, using 0.1, 1, and 10 mm path lengths quartz cuvettes. The steady-state fluorescence and excitation anisotropy spectra were measured with a PTI QuantaMaster spectrofluorimeter in 10 mm spectrofluorometric quartz cuvettes for low concentration solutions $C \leq 10^{-6}$ M. All fluorescence spectra were corrected for the spectral responsivity of the PTI detection system. The excitation anisotropy spectra were obtained in L- format configuration geometry[31] with the extraction of pure solvent emission and scattered light. The fundamental anisotropy values, r_0, were determined in viscous solution, polyTHF (pTHF), at room temperature, where the rotational correlation time, $\theta \gg \tau$ (τ is the molecular fluorescence lifetime), and the experimentally observed anisotropy was $r = r_0/(1+\theta/\tau) \approx r_0$.[31] The values of fluorescence quantum yields, Φ, were obtained in low concentration solutions by a standard method relative to 9,10 diphenylanthracene in cyclohexane (Φ ≈0.95) at room temperature.[31]

Fluorescence lifetimes of **1** were determined with a time-correlated single photon counting system PicoHarp 300 under 76 MHz femtosecond laser excitation (MIRA 900, Coherent) with the instrument response function (IRF) ≈80 ps (FWHM). Linear polarization of the laser beam was oriented by the magic angle, while the concentration in 10 mm quartz cells was $C \leq 2 \cdot 10^{-6}$ M. The quantum yields of the photochemical decomposition of **1** under one-photon excitation, Φ_{1PA}, were obtained by a previously described absorption method,[32] using 405 nm cw laser diode irradiation with average power ≈50 mW.

2.3. Two-photon measurements

The degenerate 2PA spectra of **1** and metal-ligand complexes were measured in THF and an aqueous mixture of water/ACN (1:1) over a broad spectral region by the relative 2PF method.[28] Rhodamine B in methanol, whose comprehensive characterization has been reported,[33, 34] was used as a standard. Two-photon induced fluorescence spectra were obtained with a PTI QuantaMaster spectrofluorimeter coupled with a femtosecond Clark-MXR CPA-2010 laser pumped optical parametric generator/amplifier (TOPAS). This laser system generates ≈140 fs pulses (FWHM) at a 1 kHz repetition rate. The tuning range of 600–940 nm and pulse energies $E_p \leq 0.15$ μJ were used. Fluorescence measurements were performed in 10 mm fluorometric quartz cuvettes with dye concentrations ~$(1–2) \cdot 10^{-5}$ M. The values of 2PA cross sections, δ_{2PA}, were determined by the expression:[28]

$$\delta_{2PA}^{S} = \delta_{2PA}^{R} \cdot \frac{\langle F(t) \rangle_S \cdot C_R \cdot \phi_R \cdot \Phi_R \cdot \langle P(t) \rangle_R^2}{\langle F(t) \rangle_R \cdot C_S \cdot \phi_S \cdot \Phi_S \cdot \langle P(t) \rangle_S^2},$$

where $\langle F(t) \rangle$ C, ϕ, Φ,, and $\langle P(t) \rangle$ are the average integrated fluorescence intensity, molecular concentration, geometric factor, fluorescence quantum yield, and excitation power, respectively. Subscripts *S* and *R* correspond to the sample and reference. The quadratic dependence of 2PF intensity on the excitation power was verified for each excitation wavelength, λ_{ex}. No spectral dependence $\Phi = f(\lambda_{ex})$ was observed for **1** in all solvents utilized in 2PA measurements.

3. Analytical model and quantum chemical calculations

3.1. Complexation analysis

The formation of the 1:1 ligand:metal complex in solution can be described by the equation:[35]

$$[DM] = K \cdot [D] \cdot [M], \quad (1)$$

where [*DM*] is the equilibrium concentration of complex, [*D*] and [*M*] are the concentration of ligand (dye) molecules and free metal ions, respectively, and *K* is the binding constant. Taking into account that [*D*] = *D* − [*DM*] and [*M*] = *M* − [*DM*] (*D* and *M* are the total concentrations of ligand and metal ions, respectively), eq. (1) can be rewritten as:

$$[DM] = K \cdot (D - [DM]) \cdot (M - [DM]). \quad (2)$$

The solution of eq. (2) gives:[36]

$$[DM]=\frac{\alpha(D,M)}{2}=\frac{\Delta A(\lambda)}{L\cdot\Delta\varepsilon(\lambda)}, \tag{3}$$

where $\alpha(D,M)=\left[\frac{1}{K}+D+M-\sqrt{\left(\frac{1}{K}+D+M\right)^2-4\cdot D\cdot M}\right]$, $\Delta A(\lambda)$ is the change in absorbance of the solution at a particular wavelength, λ, L is the path length of the cuvette, and $\Delta(\lambda) = \varepsilon_D(\lambda) - \varepsilon_{DM}(\lambda)$ is the difference in the extinction coefficients between pure ligand $\varepsilon_D(\lambda)$ and ligand:metal complex $\varepsilon_{DM}(\lambda)$ at the same λ. The value of binding constant K was obtained from the fitting of the experimental dependence $\Delta A = f(M)$ by eq. (3). In the case of low ligand absorption sensitivity on metal ion binding processes, changes in the corresponding fluorescence spectrum can be utilized for the determination of K. In this case, the equilibrium 1:1 ligand:metal complex concentration can be expressed as:

$$[DM]=M+\frac{F-F_0}{K\cdot(F-F^{\max})}, \tag{4}$$

where, F_0 and $F^{\max}$ are the relative fluorescence intensity of the solution at a particular wavelength, λ, for $M = 0$ and $M \gg D$, respectively. From eqs. (3) and (4) one can find:

$$\frac{F}{F_0}=\frac{1+(F^{\max}/F_0)\cdot K\cdot[\alpha(D,M)/2]}{1+K\cdot[\alpha(D,M)/2]}. \tag{5}$$

In the case of fluorescence measurements, the value of binding constant K can be determined from the fitting of the experimental dependence $\frac{F}{F_0}=f(M)$ by eq. (5). It should be mentioned that this complexation analysis is not restricted by the frequently used assumption $[M] \approx M$[9, 35, 36] and includes a full range of metal concentration.

3.2. Quantum chemical calculations

The electronic properties of free ligand and 1:1 ligand:metal complex were analyzed by quantum chemical calculations using Gaussian 2009, Rev. A2 suite of programs.[37] To save computer time, aliphatic side chains in the calculated molecules were replaced with methyl groups. This is a reasonable approach since the substituents in the 9-position of the fluorene ring are not in conjugation with the aromatic system and exhibit no substantial effect on the electronic distribution of the chromophore system.[38] The ground-state geometries of **1** and **1**:Zn^{2+} were optimized using DFT with the B3LYP exchange-correlation functional and the standard 6-31G* basis set. Initial (before optimization) structures of **1** and **1**:Zn^{2+} were constructed using X-ray crystal data for a dibenzosubstituted oxaaza macrocycle reported previously.[27] Because the experiment was carried out in a polar solvent (THF) and aqueous solution (water/ACN), the THF parameters were used with the Polarizable Continuum model (PCM) for geometry optimization and simulation of excitations. The permanent and state-to-state transition dipoles were obtained using *a posteriori* Tamm-Dancoff approximation (ATDA),[39] implemented in a locally modified version of the Gaussian 2009 code. The values of 1PA and 2PA cross sections were calculated at the TD-B3LYP/6-31G* level of theory and the Sum-Over-States expressions[40] with the empirical damping parameter $\Gamma = 0.1$eV.

4. Results and discussion

4.1. Synthesis

Fluorene-based chemosensor probe **1** (Figure 1) is comprised of a fluorenyl π-electron bridge with an unsymmetrical chemical structure. Figure 1 illustrates the strategy used to incorporate an oxaaza macrocyclic ligand containing an amine terminal pendant arm to the fluorenyl 2-position via an addition reaction. The synthesis of the oxaaza macrocyclic ligand **B** was derived from cyclocondensation of O^1,O^7-bis(2-formylphenyl)-1,4,7-trioxaheptane and diethylenetriamine in methanol, followed by an *in situ* reduction using $NaBH_4$, as described in Ref [37]. Details of the synthesis and characterization of fluorene isothiocyanate was previously reported.[30] Conjugation reaction between the oxaaza macrocyclic ligand and the isothiocyanate fluorene reactive probe was carried out in DMF under N_2 at room temperature. Full characterization, including ^1H and ^{13}C NMR, and HR-MS analysis, confirmed the molecular structure of **1**. In the ^{13}C NMR spectrum, the thiocarbonyl carbon signal was observed at 180.7 ppm. Additionally, FT-IR analysis revealed the disappearance of the strong −NCS stretch at 2111 cm^{-1} present in fluorene isothiocyanate **C** precursor.

4.2. Linear photophysical properties

Probe **1** is an unsymmetrical fluorene-based molecule containing a dibenzosubstituted oxaaza macrocycle, a metal ion binding construct.[27, 41] The conjugation length of **1** was increased via the addition of a polarizable π-system (styryl) between the fluorenyl moiety and the benzothiazole acceptor group. In the 7-position, thiourea NH moiety acts as electron-donating group. The steady-state absorption spectra of **1** were nearly independent of solvent properties (Figure 2a, curves 1–5), with small changes (≤ 10 %) in the corresponding maxima extinction coefficients ε^{max} (Table 1). In contrast, the steady-state fluorescence spectra (Fig. 2a, curves 1′-5′) exhibited a strong solvatochromic behavior associated with an increase in the stationary dipole moment of **1** upon electronic excitation, typical for unsymmetrical fluorene derivatives.[42, 43] The values of the Stokes shifts increased up to 157 nm (in DMSO), while no strict correspondence to the Lippert equation[31] was observed. Excitation anisotropy spectra of **1** (Figure 2b, curves 1, 2) revealed the nature of the main 1PA band. A nearly constant value of anisotropy $r(\lambda)$ over the 340–430 nm spectral range corresponded to one electronic transition $S_0 \rightarrow S_1$ (S_0 and S_1 are the ground and first excited electronic states of **1**, respectively). In viscous pTHF, $r \approx r_0$ and relatively high values of anisotropy in the main absorption band were observed, $r_0 \approx 0.35$, corresponding to a small angle (< 20°) between absorption ($S_0 \rightarrow S_1$) and emission ($S_1 \rightarrow S_0$) transition dipole moments. This allows one to estimate that the transition dipoles $S_0 \rightarrow Sn$ (Sn, n = 0, 1, 2, 3, ….) have mutual orientations.[31] The values of fluorescence quantum yields were sufficiently high (Φ > 0.5), and exhibited a weak and complicated dependence on solvent properties with no correlation with solvent polarity Δf (see Table 1).

Fluorescence lifetimes corresponded to a single-exponential decay process with the observed values in the range of $1.0 < \tau < 1.7$ ns, gradually increasing with Δf. The unique characteristics of the linear photophysical parameters of **1** in a number of organic solvents allow one to assume noticeable changes in its equilibrium molecular geometry and electronic structure in the S_1 state.

The photostability of **1** under one-photon excitation in the main long wavelength absorption band was determined, resulting in the photochemical quantum yield $10^{-4} \leq \Phi_{1PA} \leq 7 \cdot 10^{-4}$ (see Table 1) that noticeably depended on the nature of the medium. The highest level of photostability was observed for **1** in DMSO ($\Phi_{1PA} \approx 10^{-4}$) and substantially decreased in ACN ($\Phi_{1PA} \approx 6.3 \cdot 10^{-4}$). A comparative analysis of the obtained and known values of

Φ_{1PA}[44, 45] indicated that photostability of the new fluorene-based macrocyclic probe **1** is reasonably high and suitable for practical applications.

4.3. Sensing properties

The investigation of metal ion sensing behavior of **1** was performed in THF and water/ACN (1:1) solutions. The addition of Zn^{2+} ions to THF solution of **1** resulted in visible changes in the absorption and fluorescence spectra (Figure 3a, b). The increase of total ion concentration [Zn^{2+}] from $2{\cdot}10^{-6}$ to $2.4{\cdot}10^{-4}$ M in the $2.5{\cdot}10^{-5}$ M THF solution of **1** led to a hypsochromic shift in the absorption spectrum to 381 nm and ≈10 % increase in extinction coefficient (see Figure 3a and Table 2). Well defined isobestic points are indicative of the presence of only two absorbing species. Under the highest metal ion concentration, [Zn^{2+}] ≈$2.4{\cdot}10^{-4}$ M, nearly all ligand molecules were in the complexed form and no changes in absorption were observed for additional increase in [Zn^{2+}].

The dependence of the change in absorbance ΔA at 360 nm as a function of [Zn^{2+}] (Figure 3c) can be reasonably fit by eq. (3), indicative of 1:1 ligand:metal complex formation (i.e. a single- step complexation equilibrium). The value of binding constant $K \approx (3 \pm 0.3) \cdot 10^5$ M^{-1} corresponded to the best fit of experimental dependence $\Delta A = f(M)$. The fluorescence spectrum of **1** in THF ($D \approx 2{\cdot}10^{-6}$ M) exhibited a hypsochromic shift up to 30 nm with an increase in intensity upon addition of Zn^{2+} in concentrations up to $2.4{\cdot}10^{-5}$ M (Figure 3b). A sharp isobestic point and a single-exponential fluorescence decay process for the highest Zn^{2+} concentration (see Table 2) were consistent with 1:1 ligand:metal complex formation and nearly full conversion of ligand molecules into the complexed form. The analysis of the ratio of fluorescence intensities from the solution with ligand:metal mixture at 420 and 650 nm, F_S, revealed good selectivity to Zn^{2+} ions with a relatively large dynamic range (see Figure 3d), spanning 1×10^{-4} to 1×10^{-6} M, useful for ratiometric measurements of biologically-relevant concentrations.[6, 35] It should be mentioned that fluorene- based probe **1** did not exhibit comparable selectivity to Mg^{2+}, Ca^{2+}, and K^+ ions under the same experimental conditions.

The fluorescence spectrum of **1** in aqueous solution (water/ACN (1:1)) revealed noticeable changes under the addition of Zn^{2+} ions (Figure 4a), as was the case in organic solvent. In contrast, the absorption spectrum of **1** was nearly insensitive to the Zn^{2+} ion bonding in aqueous medium (Figure 5b). In this case, the fluorescence spectra of **1** ($D \approx 1.7{\cdot}10^{-6}$ M) were obtained for the range of Zn^{2+} concentrations from $1.7{\cdot}10^{-7}$ M to $2.0{\cdot}10^{-4}$ M. The change in relative fluorescence intensity $\frac{F}{F_0}$ at 460 nm as a function of [Zn^{2+}] is presented in Figure 4b (circles) and can be reasonably fitted by eq. (5) (solid line) with the corresponding binding constant $K \approx (2 \pm 0.2){\cdot}10^5$ M^{-1}. The experimentally obtained data along with the main photophysical parameters (see Table 2) are consistent with 1:1 ligand:metal complex formation and full transformation of ligand molecules into the complexed form under the highest concentration of Zn^{2+} used.

The values of fluorescence quantum yield Φ and lifetimes τ for **1**:Zn^{2+} complex in THF decreased by 15–20 % in comparison with those of the corresponding pure ligand (see Tables 1, 2). In contrast, water/ACN solution of **1** with mixtures of Zn^{2+} exhibited a small increase (by ≈ 10 %) in the fluorescence quantum yield which is not consistent with corresponding observed trend in τ.[31] Excitation anisotropy spectra of **1** and **1**:Zn^{2+} complexes in THF and aqueous solutions (Figure 5a, b) exhibited a close spectral dependence that is indicative of their similar mutual orientations of the transition dipoles $S_0 \rightarrow S_1$ and $S_0 \rightarrow Sn$ (n = 1, 2, 3…). A comprehensive analysis of the main photophysical data revealed a rather complex nature of the influence of Zn^{2+} ion binding processes on the electronic structure of **1**. We believe that the mechanism of sensing is based on the

coordination of the macrocyclic receptor to the Zn^{2+}. This process results in perturbation of the electronic environment of the chromophore by decreasing basicity of the receptor nitrogens.

The photochemical stability of **1** in THF and water/ACN solution exhibited a specific dependence on Zn^{2+} (see Table 2). The photochemical decomposition quantum yield Φ_{1PA} of the **1**:Zn^{2+} complex in THF increased by a factor of ≈2 relative to the pure ligand. In contrast, the photostabilities of **1** and ligand:metal complex in water/ACN (1:1) were nearly the same, with only a small increase in Φ_{1PA} upon metal ion binding. Thus, probe **1** demonstrated high photostability, suitable for fluorometirc sensing, and particularly important for potential *in vivo* imaging and sensing applications.

4.4. 2PA properties of 1 and 1:Zn^{2+} complex

The degenerate 2PA spectra of **1** and **1**:Zn^{2+} complexes were investigated by the relative 2PF method[28] with 1 kHz femtosecond laser system in organic and aqueous media. All nonlinear absorption measurements of **1**:Zn^{2+} complexes were performed on solutions with $M \gg D$, where only 1:1 bound ligand molecules were present. The 2PA spectra (Figure 6) were characterized by two well-defined short and long wavelength bands, with the maximum at λ_{ex}/**2** = 320–330 nm and 390–400 nm, respectively. The long wavelength 2PA band overlapped quite well with the main 1PA band which is typical for unsymmetrical fluorene derivatives.[46–48] This band was characterized by maximum 2PA cross section δ_{2PA} ≈130 GM for **1** in THF and decreased by a factor of ≈2 upon Zn^{2+} binding (Figure 6, curves 1, 1′). In contrast, nearly the same values of δ_{2PA} ≈50 GM were observed for **1** and **1**:Zn^{2+} complex in water/ACN solution (Figure 6, curves 2, 2′). Well-defined long wavelength 2PA bands in the spectral range of one-photon allowed transitions are associated with the relatively large changes in the stationary dipole moments of the ligand and ligand:metal complex ($|\mathbf{\Delta\mu}|$ ~ 5 – 10 D) under the $S_0 \rightarrow S_1$ electronic excitation.[48–50] The values of 2PA cross sections of **1** in the shorter wavelength (higher energy) two-photon allowed band (λ_{ex}/2 = 320–330 nm) corresponded to ≈240 and ≈140 GM in THF and water/ACN solution, respectively. The addition of Zn^{2+} to the THF solution of **1** resulted in ≈30 % decrease in δ_{2PA}. In contrast, nearly the reverse effect (but same magnitude of change) was observed for **1** in water/ACN solution, i.e., a higher 2PA cross section was observed for the complex relative to free ligand. It should also be mentioned that the corresponding behavior of the two-photon action cross sections $\delta_{2PA} \cdot \Phi$ upon complexation were sufficiently close to the values of δ_{2PA} due to only a small change in the fluorescence quantum yield upon metal binding. The maximum values of $\delta_{2PA} \cdot \Phi$ ≈(90–130) GM for **1**:Zn^{2+} complexes are suitable for application in 2PFM techniques.

4.5. Quantum chemical calculations for 1 and 1:Zn^{2+} complex

The crystal structure of dibenzosubstituted oxaaza macrocycle[27] reveals Zn^{2+} coordinated to the four nitrogens of the ligand. The corresponding optimized molecular geometries for the model compounds of **1** (**1a**) and **1**:Zn^{2+} (**2a**) are presented in Figure 7. The calculated molecular orbitals (Figure 7) demonstrate weak polarization of the highest occupied molecular orbital upon metal binding, resulting in 5–10% decrease in the absolute values of transition dipoles from **1a** to **2a**. However their spatial orientations (see values of the relative angle, α, for the main electronic transitions in Table 3) remain close. This result is in good agreement with experimental anisotropy spectra (Figure 5) which are nearly identical for **1** and the **1**:Zn^{2+} complex. Calculated energies of the electronic transitions and 2PA cross sections predict a weak dependence on metal ion binding (Table 3) which is also consistent with experimental data. The absolute values of δ_{2PA} exhibit a relatively large deviation from the corresponding experimental parameters. This may be due to more complicated nature of

specific solvation and metal-ligand coordinating processes, a question that is presently under investigation.

5. Conclusions

Linear photophysical, photochemical, 2PA, and metal ion sensing properties of a new fluorene-based probe **1** containing a dibenzosubstituted oxaaza macrocycle were investigated in organic and aqueous solution as a potential Zn^{2+} sensor for two-photon bioimaging and sensing applications. The steady-state absorption spectra of unsymmetrical **1** were nearly independent of solvent properties, while a strong solvatochromic effect was observed in the fluorescence spectra without dramatic changes in the fluorescence quantum yield. The values of fluorescence lifetimes corresponded to a single-exponential decay and exhibited a weak dependence on solvent polarity. The addition of Zn^{2+} to organic and aqueous solutions of **1** resulted in noticeable changes in absorption and fluorescence spectra, consistent with a 1:1 complexation mechanism with sufficiently high binding constants $K \sim (2 – 3)\cdot 10^5\ M^{-1}$, in contrast to other metal ions, such as Mg^{2+}, Ca^{2+}, and K^+. The photochemical stability of **1** and the **1**:Zn^{2+} complex was investigated by determining the corresponding photodecomposition quantum yields, Φ_{1PA}, and were in the range $(1 < \Phi_{1PA} < 7)\cdot 10^{-4}$. The values of Φ_{1PA} exhibited a complex dependence on solvent properties and increased slightly upon metal ion binding. The 2PA spectra of **1** and the **1**:Zn^{2+} complex were characterized by two well defined absorption bands at ≈650 and 800 nm with maxima cross sections $\delta_{2PA} \approx$ 140–240 GM and 50–130 GM, respectively. The electronic properties of the 2PA bands of **1** and **1**:Zn^{2+} complexes were analyzed based on computational results while a weak dependence of 2PA efficiency on complexation was shown. The high sensitivity and selectivity of the new fluorenyl macrocycle **1** to Zn^{2+} along with excellent ratiometric fluorescence detection parameters, good photochemical stability, and a relatively large two-photon action cross section (90–130 GM) for the **1**:Zn^{2+} complex suggests **1** may be potentially useful as a Zn ion sensor in 2PFM bioimaging, a subject of future work.

Acknowledgments

We wish to acknowledge the Civilian Research and Development Foundation (UKB2-2923-KV-07), the Ministry of Education and Science of Ukraine (grant M/49-2008), the National Science Foundation (CHE-0832622 and CHE-0840431), and the National Institutes of Health (1 R15 EB008858-01) for support of this work.

References

1. Chen XY, Shi J, Li YM, Wang FL, Wu X, Guo QX, Liu L. Two-Photon Fluorescent Probes of Biological Zn(II) Derived from 7-Hydroxyquinoline. Organic Letters. 2009; 11(19):4426–4429. [PubMed: 19722549]
2. Dong XH, Yang YY, Sun J, Liu ZH, Liu BF. Two-photon excited fluorescent probes for calcium based on internal charge transfer. Chemical Communications. 2009; (26):3883–3885. [PubMed: 19662240]
3. Mank M, Santos AF, Direnberger S, Mrsic-Flogel TD, Hofer SB, Stein V, Hendel T, Reiff DF, Levelt C, Borst A, Bonhoeffer T, Hubener M, Griesbeck O. A genetically encoded calcium indicator for chronic in vivo two-photon imaging. Nature Methods. 2008; 5(9):805–811. [PubMed: 19160515]
4. Svoboda K, Yasuda R. Principles of two-photon excitation microscopy and its applications to neuroscience. Neuron. 2006; 50(6):823–839. [PubMed: 16772166]
5. Ha-Thi MH, Penhoat M, Drouin D, Blanchard-Desce M, Michelet V, Leray I. Synthesis, fluorescence, and two-photon absorption of bidentate phosphane oxide derivatives: Complexation with Pb2+ and Cd2+ cations. Chemistry-a European Journal. 2008; 14(19):5941–5950.
6. Sumalekshmy S, Henary MM, Siegel N, Lawson PV, Wu Y, Schmidt K, Bredas JL, Perry JW, Fahrni CJ. Design of emission ratiometric metal-ion sensors with enhanced two-photon cross

section and brightness. Journal of the American Chemical Society. 2007; 129(39):11888. [PubMed: 17845038]

7. Tian YQ, Chen CIY, Yang CC, Young AC, Jang SH, Chen WC, Jen AKY. 2-(2 ′-Hydroxyphenyl)benzoxazole-containing two-photon-absorbing chromophores as sensors for zinc and hydroxide ions. Chemistry of Materials. 2008; 20(5):1977–1987.
8. Ahn HC, Yang SK, Kim HM, Li SJ, Jeon SJ, Cho BR. Molecular two-photon sensor for metal ions derived from bis(2-pyridyl)amine. Chemical Physics Letters. 2005; 410(4–6):312–315.
9. Pond SJK, Tsutsumi O, Rumi M, Kwon O, Zojer E, Bredas JL, Marder SR, Perry JW. Metal-ion sensing fluorophores with large two-photon absorption cross sections: Aza-crown ether substituted donor-acceptor-donor distyryl benzenes. Journal of the American Chemical Society. 2004; 126(30): 9291–9306. [PubMed: 15281820]
10. Kuba K, Nakayama S. Two-photon laser-scanning microscopy: tests of objective lenses and Ca2+ probes. Neuroscience Research. 1998; 32(3):281–294. [PubMed: 9875569]
11. Rivet S, Canioni L, Sarger L, Barille R, Vacher P, Ducret T. Visualization of intracellular CA(2+) dynamics with simultaneous 2-photon excited fluorescence and third harmonic generation microscope. Journal of Fluorescence. 2002; 12(2):197–199.
12. Rose CR, Kovalchuk Y, Eilers J, Konnerth A. Two-photon Na+ imaging in spines and fine dendrites of central neurons. Pflugers Archiv-European Journal of Physiology. 1999; 439(1–2): 201–207. [PubMed: 10651018]
13. Nguyen QT, Callamaras N, Hsieh C, Parker I. Construction of a two-photon microscope for video-rate Ca2+ imaging. Cell Calcium. 2001; 30(6):383–393. [PubMed: 11728133]
14. Micu I, Ridsdale A, Zhang LQ, Woulfe J, McClintock J, Brantner CA, Andrews SB, Stys PK. Real-time measurement of free Ca2+ changes in CNS myelin by two-photon microscopy. Nature Medicine. 2007; 13(7):874–879.
15. Kim HM, Jeong MY, Ahn HC, Jeon SJ, Cho BR. Two-photon sensor for metal ions derived from azacrown ether. Journal of Organic Chemistry. 2004; 69(17):5749–5751. [PubMed: 15307750]
16. Domaille DW, Que EL, Chang CJ. Synthetic fluorescent sensors for studying the cell biology of metals. Nature Chemical Biology. 2008; 4(3):168–175.
17. Chen Y, Pu KY, Fan QL, Qi XY, Huang YQ, Lu XM, Huang W. Water-Soluble Anionic Conjugated Polymers for Metal Ion Sensing: Effect of Interchain Aggregation. Journal of Polymer Science Part a-Polymer Chemistry. 2009; 47(19):5057–5067.
18. Kennedy DP, Kormos CM, Burdette SC. FerriBRIGHT: A Rationally Designed Fluorescent Probe for Redox Active Metals. Journal of the American Chemical Society. 2009; 131(24):8578–8586. [PubMed: 19459701]
19. Lin WY, Yuan L, Cao XW, Tan W, Feng YM. A Coumarin-Based Chromogenic Sensor for Transition-Metal Ions Showing Ion-Dependent Bathochromic Shift. European Journal of Organic Chemistry. 2008(29):4981–4987.
20. Hyrc KB, Bownik JM, Goldberg MP. Ionic selectivity of low-affinity ratiometric calcium indicators: mag-Fura-2, Fura-2FF and BTC. Cell Calcium. 2000; 27(2):75–86. [PubMed: 10756974]
21. Ricci AJ, Wu YC, Fettiplace R. The endogenous calcium buffer and the time course of transducer adaptation in auditory hair cells. Journal of Neuroscience. 1998; 18(20):8261–8277. [PubMed: 9763471]
22. Frederickson CJ. Neurobiology of Zinc and Zinc-Containing Neurons. International Review of Neurobiology. 1989; 31:145–238. [PubMed: 2689380]
23. Ueno T, Urano Y, Setsukinai K, Takakusa H, Kojima H, Kikuchi K, Ohkubo K, Fukuzumi S, Nagano T. Rational principles for modulating fluorescence properties of fluorescein. Journal of the American Chemical Society. 2004; 126(43):14079–14085. [PubMed: 15506772]
24. Bhaskar A, Ramakrishna G, Twieg RJ, Goodson T. Zinc sensing via enhancement of two-photon excited fluorescence. Journal of Physical Chemistry C. 2007; 111(40):14607–14611.
25. Kim HM, Seo MS, An MJ, Hong JH, Tian YS, Choi JH, Kwon O, Lee KJ, Cho BR. Two-photon fluorescent probes for intracellular free zinc ions in living tissue. Angewandte Chemie-International Edition. 2008; 47(28):5167–5170.

26. Henary MM, Wu YG, Fahrni CJ. Zinc(II)-selective ratiometric fluorescent sensors based on inhibition of excited-state intramolecular proton transfer. Chemistry-a European Journal. 2004; 10(12):3015–3025.
27. Vicente M, Bastida R, Lodeiro C, Macias A, Parola AJ, Valencia L, Spey SE. Metal complexes with a new N4O3 amine pendant-armed macrocyclic ligand: Synthesis, characterization, crystal structures, and fluorescence studies. Inorganic Chemistry. 2003; 42(21):6768–6779. [PubMed: 14552629]
28. Albota MA, Xu C, Webb WW. Two-photon fluorescence excitation cross sections of biomolecular probes from 690 to 960 nm. Applied Optics. 1998; 37(31):7352–7356. [PubMed: 18301569]
29. Adam KRL, AJ, Lindoy LF, Lip HC, Skelton BW, White AH. Ligand design and metal-ion recognition. Interaction of nickel(11) with 17- to 19-membered macrocycles containing 02N3 and 03N2 donor sets and the x-ray structure of the parent 17-membered macrocyclic ligand. Journal of the American Chemical Society. 1983; 105:4645–4661.
30. Morales AR, Schafer-Hales KJ, Marcus AI, Belfield KD. Amine-Reactive Fluorene Probes: Synthesis, Optical Characterization, Bioconjugation, and Two-Photon Fluorescence Imaging. Bioconjugate Chemistry. 2008; 19(12):2559–2567. [PubMed: 19090700]
31. Lakowicz, JR. Principles of fluorescence spectroscopy. Kluwer; New York: 1999.
32. Corredor CC, Belfield KD, Bondar MV, Przhonska OV, Yao S. One- and two-photon photochemical stability of linear and branched fluorene derivatives. Journal of Photochemistry and Photobiology a-Chemistry. 2006; 184(1–2):105–112.
33. Xu C, Webb WW. Measurement of two-photon excitation cross sections of molecular fluorophores with data from 690 to 1050 nm. Journal of the Optical Society of America B-Optical Physics. 1996; 13(3):481–491.
34. Makarov NS, Drobizhev M, Rebane A. Two-photon absorption standards in the 550–1600 nm excitation wavelength range. Optics Express. 2008; 16(6):4029–4047. [PubMed: 18542501]
35. Connors, KA. Binding constants: The measurement of molecular complex stability. John Wiley and Sons; New York: 1987.
36. Valeur B, Pouget J, Bourson J, Kaschke M, Ernsting NP. Tuning of Photoinduced Energy-Transfer in a Bichromophoric Coumarin Supermolecule by Cation Binding. Journal of Physical Chemistry. 1992; 96(16):6545–6549.
37. Frisch, MJT.; GW; Schlegel, HB.; Scuseria, GE.; Robb, MA.; Cheeseman, JR.; Scalmani, G.; Barone, V.; Mennucci, B.; Petersson, GA.; Nakatsuji, H.; Caricato, M.; Li, X.; Hratchian, HP.; Izmaylov, AF.; Bloino, J.; Zheng, G.; Sonnenberg, JL.; Hada, M.; Ehara, M.; Toyota, K.; Fukuda, R.; Hasegawa, J.; Ishida, M.; Nakajima, T.; Honda, Y.; Kitao, O.; Nakai, H.; Vreven, T.; Montgomery, JA., Jr; Peralta, JE.; Ogliaro, F.; Bearpark, M.; Heyd, JJ.; Brothers, E.; Kudin, KN.; Staroverov, VN.; Kobayashi, R.; Normand, J.; Raghavachari, K.; Rendell, A.; Burant, JC.; Iyengar, SS.; Tomasi, J.; Cossi, M.; Rega, N.; Millam, NJ.; Klene, M.; Knox, JE.; Cross, JB.; Bakken, V.; Adamo, C.; Jaramillo, J.; Gomperts, R.; Stratmann, RE.; Yazyev, O.; Austin, AJ.; Cammi, R.; Pomelli, C.; Ochterski, JW.; Martin, RL.; Morokuma, K.; Zakrzewski, VG.; Voth, GA.; Salvador, P.; Dannenberg, JJ.; Dapprich, S.; Daniels, AD.; Farkas, Ö.; Foresman, JB.; Ortiz, JV.; Cioslowski, J.; Fox, DJ. Gaussian 09, Revision A.2. Gaussian, Inc; Wallingford CT: 2009.
38. Andrasik SJ, Belfield KD, Bondar MV, Hernandez FE, Morales AR, Przhonska OV, Yao S. One- and two-photon singlet oxygen generation with new fluorene-based photosensitizers. Chemphyschem. 2007; 8(3):399–404. [PubMed: 17226876]
39. Mikhailov IATS, Masunov AE. Double excitations and state-to-state transition dipoles in pi-pi* excited singlet states of linear polyenes: Time-dependent density-functional theory versus multiconfigurational methods. Physical Review A. 2008; 77(1):012510(11).
40. Mikhailov IA, Bondar MV, Belfield KD, Masunov AE. Electronic Properties of a New Two-Photon Absorbing Fluorene Derivative: The Role of Hartree-Fock Exchange in the Density Functional Theory Design of Improved Nonlinear Chromophores. Journal of Physical Chemistry C. 2009; 113(48):20719–20724.
41. Vicente M, Bastida R, Macias A, Valencia L, Geraldes C, Brondino CD. Copper complexes with new oxaaza-pendant-armed macrocyclic ligands: X-ray crystal structure of a macrocyclic copper(II) complex. Inorganica Chimica Acta. 2005; 358(4):1141–1150.

42. Belfield KD, Bondar MV, Przhonska OV, Schafer KJ, Mourad W. Spectral properties of several fluorene derivatives with potential as two-photon fluorescent dyes. J Lumin. 2002; 97(2):141–146.
43. Belfield KD, Bondar MV, Kachkovsky OD, Przhonska OV, Yao S. Solvent effect on the steady-state fluorescence anisotropy of two-photon absorbing fluorene derivatives. J Lumin. 2007; 126(1):14–20.
44. Belfield KD, Bondar MV, Przhonska OV, Schafer KJ. One- and two-photon photostability of 9,9-didecyl-2,7-bis(N,N-diphenylamino)fluorene. Photochemical & Photobiological Sciences. 2004; 3(1):138–141. [PubMed: 14768631]
45. Belfield KD, Bondar MV, Przhonska OV, Schafer KJ. Photochemical properties of (7-benzothiazol-2-yl-9, 9-didecylfluoren-2-yl)diphenylamine under one- and two-photon excitation. Journal of Photochemistry and Photobiology a-Chemistry. 2004; 162(2–3):569–574.
46. Belfield KD, Bondar MV, Hernandezt FE, Przhonska OV, Yao S. Two-photon absorption cross section determination for fluorene derivatives: Analysis of the methodology and elucidation of the origin of the absorption processes. Journal of Physical Chemistry B. 2007; 111(44):12723–12729.
47. Morales AR, Schafer-Hales KJ, Yanez CO, Bondar MV, Przhonska OV, Marcus AI, Belfield KD. Excited State Intramolecular Proton Transfer and Photophysics of a New Fluorenyl Two-Photon Fluorescent Probe. Chemphyschem. 2009; 10(12):2073–2081. [PubMed: 19449363]
48. Belfield KD, Bondar MV, Hernandez FE, Masunov AE, Mikhailov IA, Morales AR, Przhonska OV, Yao S. Two-Photon Absorption Properties of New Fluorene-Based Singlet Oxygen Photosensitizers. Journal of Physical Chemistry C. 2009; 113(11):4706–4711.
49. Ohta K, Antonov L, Yamada S, Kamada K. Theoretical study of the two-photon absorption properties of several asymmetrically substituted stilbenoid molecules. Journal of Chemical Physics. 2007; 127(8)
50. Belfield KD, Bondar MV, Yanez CO, Hernandez FE, Przhonska OV. Two-photon absorption and lasing properties of new fluorene derivatives. Journal of Materials Chemistry. 2009; 19(40):7498–7502.

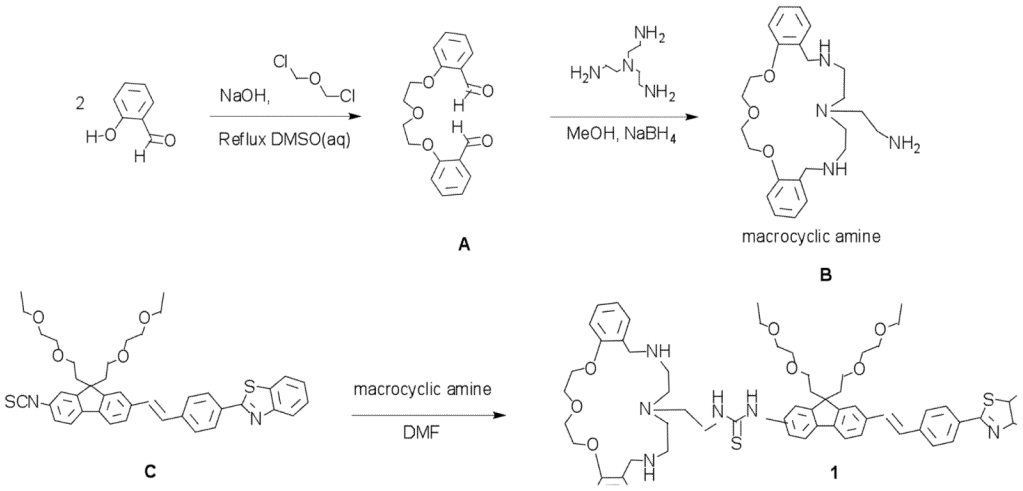

Figure 1.
Synthesis of fluorene-based chemosensor **1**.

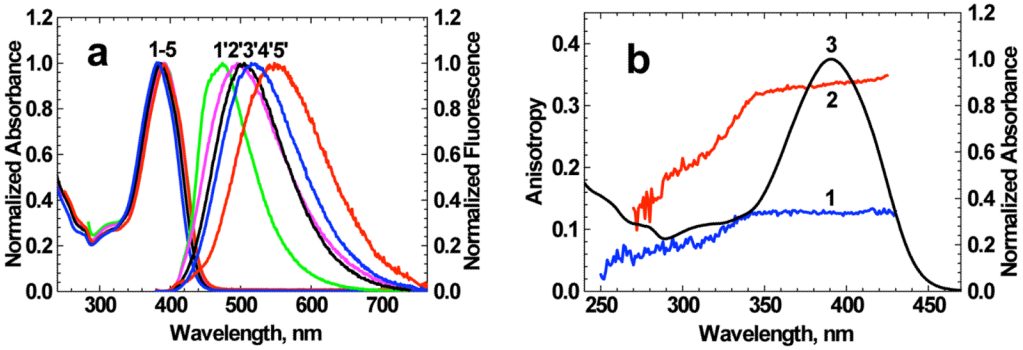

Figure 2.

(a) Normalized linear absorption (1–5) and fluorescence (1′-5′) spectra of **1** in toluene (1′), THF (2′), DCM (3′) ACN (4′) and DMSO (5′). (b) Excitation anisotropy spectra of **1** in THF (1) and pTHF (2) (observed wavelengths correspond to the fluorescence maxima) and normalized linear absorption spectrum in THF (3).

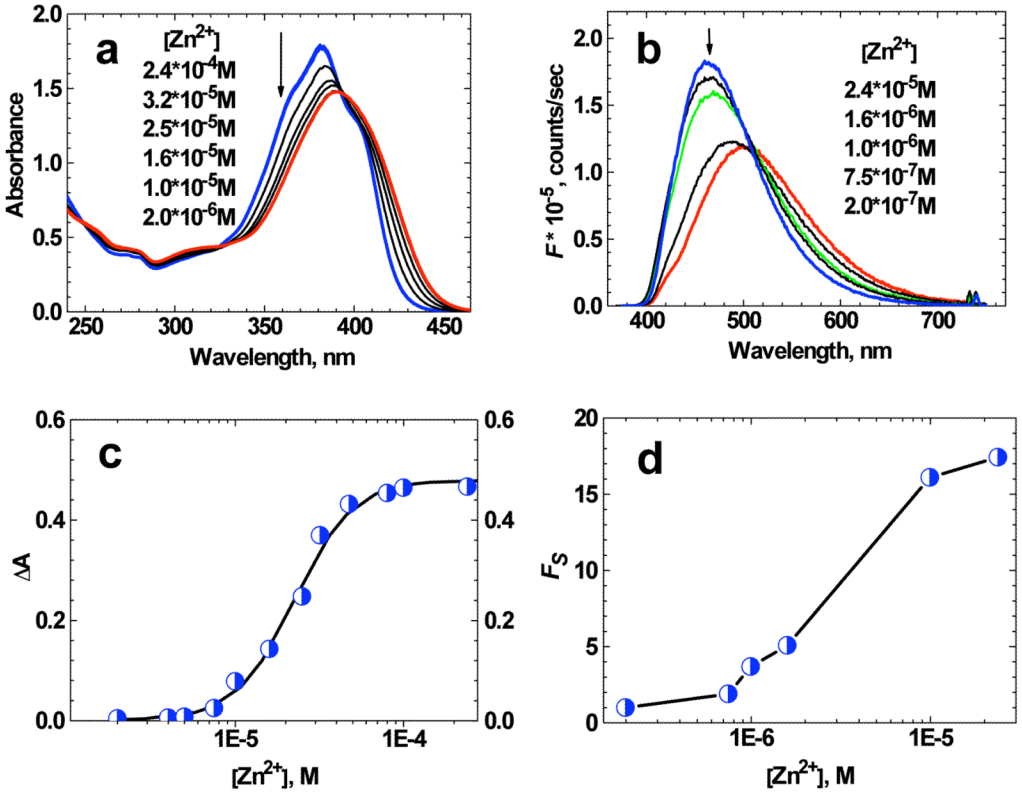

Figure 3.

(a) Absorption spectra of **1** in THF (***D*** ≈ 2.5·10^{-5} M) for different values of total ion concentration [Zn^{2+}]. (b) Fluorescence spectra of **1** in THF (***D*** ≈ 2·10^{-6} M) for different values of [Zn^{2+}] (λ_{ex} = 370 nm). The arrows indicate the decrease in [Zn^{2+}]. (c) Change in absorbance at 360 nm as a function of [Zn^{2+}] for **1** in THF (***D*** ≈ 2.5·10^{-5} M). The solid line corresponds to the best fit by eq. (3). (d) Dependence $F_s = f([Zn^{2+}])$ for **1** in THF (***D*** ≈ 2·10^{-6} M). The absolute accuracy of each experimental point is ±10%.

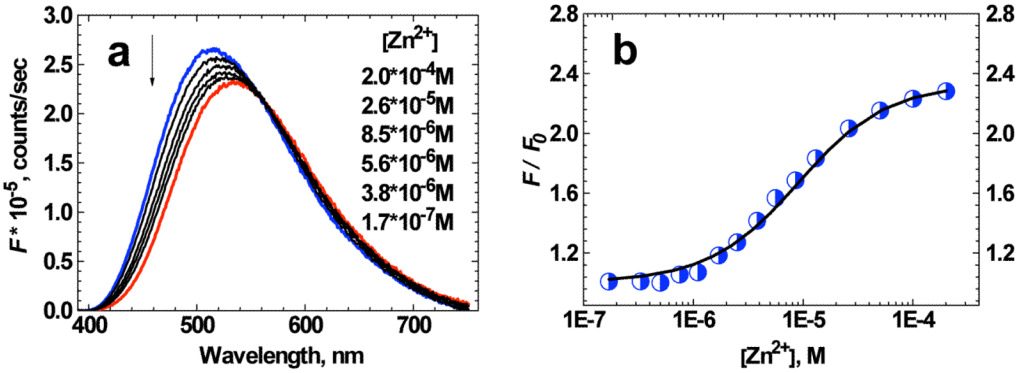

Figure 4.

(a) Fluorescence spectra of **1** in water/ACN (1:1) solution (***D*** ≈ 1.7·10^{-6} M) as a function of [Zn^{2+}]. The arrow indicates decreasing [Zn^{2+}]. (b) Relative change in fluorescence intensity ***F*** / ***F*$_0$** at 460 nm as a function of [Zn^{2+}] for **1** in water/ACN (1:1) solution (***D*** ≈ 1.7·10^{-6} M). The solid line corresponds to the best fit by eq. (5). The absolute accuracy of each experimental point is ± 10%.

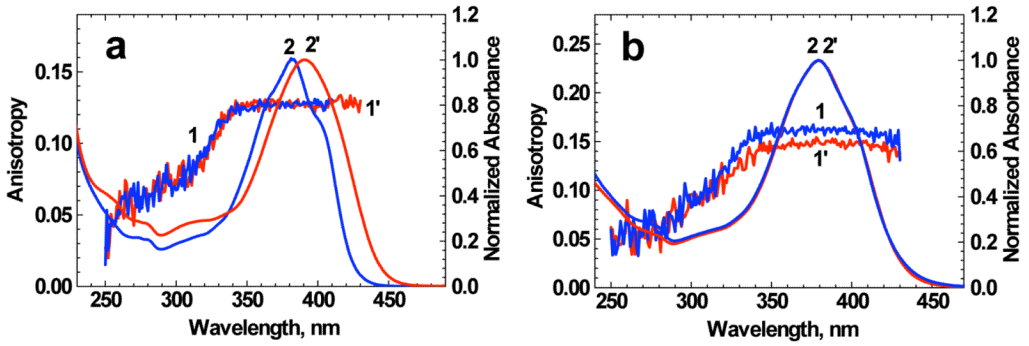

Figure 5.

Excitation anisotropy (1, 1′) and normalized linear absorption (2, 2′) spectra of **1** (1′, 2′) and **1**:Zn^{2+} complexes (1, 2) in THF (a) and water/ACN (1:1) (b).

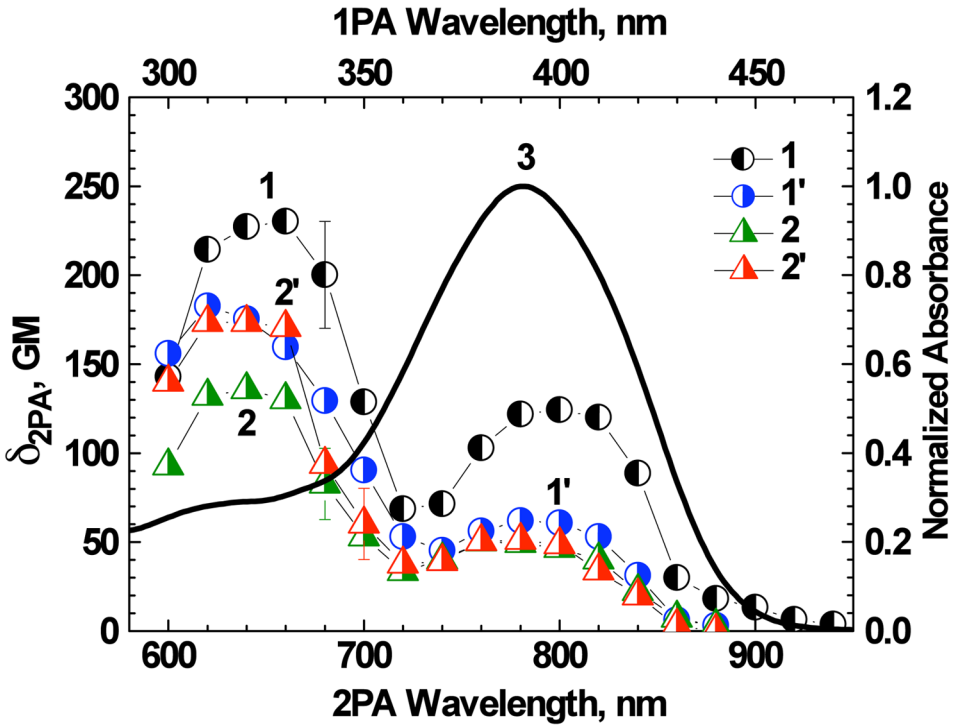

Figure 6.

2PA spectra of **1** (1, 2) and **1**:Zn^{2+} complex (1′, 2′) in THF (1, 1′) and water/ACN (1:1) (2, 2′). Normalized linear absorption spectrum of **1** in THF (3). Total concentrations of **1** and Zn^{2+} ions in solution were $1.2 \cdot 10^{-5}$ M and $8 \cdot 10^{-4}$ M, respectively.

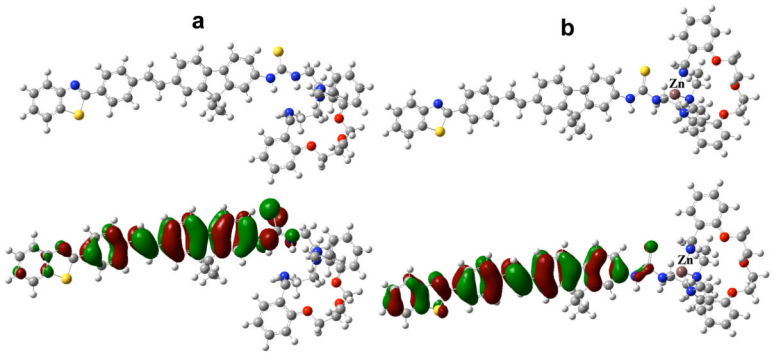

Figure 7.
Optimized molecular geometry (upper), and highest occupied molecular orbitals (lower) of model compounds **1a** (a) and **2a** (b).

Table 1

Linear photophysical and photochemical parameters of **1** in organic solvents of different polarity Δf [*]: absorption λ_{abs}^{max} and fluorescence λ_{fl}^{max} maxima, Stokes shifts, maximum extinction coefficients ε^{max}, fluorescence quantum yields Φ and lifetimes τ, quantum yields of photochemical decomposition under one-photon irradiation Φ_{1PA}.

N/N	Toluene	THF	DCM	DMSO	ACN
Δf	0.0135	0.209	0.217	0.263	0.305
λ_{abs}^{max}, nm	391 ± 1	391 ± 1	386 ± 1	391 ± 1	382 ± 1
λ_{fl}^{max}, nm	473 ± 1	496 ± 1	504 ± 1	548 ± 1	517 ± 1
Stokes shift, cm^{-1}	4430 ± 100	5410 ± 100	6070 ± 100	7330 ± 100	6840 ± 100
$\varepsilon^{max} \cdot 10^{-3}$, $M^{-1} \cdot cm^{-1}$	-	61 ± 3	59 ± 3	58 ± 3	56 ± 3
Φ	0.72 ± 0.04	0.83 ± 0.05	0.94 ± 0.05	0.54 ± 0.03	0.78 ± 0.04
τ, ns[**]	1.08 ± 0.08	1.44 ± 0.08	1.45 ± 0.08	1.59 ± 0.08	1.63 ± 0.08
$\Phi_{1PA} \cdot 10^4$	-	1.6 ± 0.4	2.0 ± 0.4	1.0 ± 0.3	6.3 ± 2

[*] orientation polarizability $\Delta f = (\varepsilon - 1)/(2\varepsilon + 1) - (n^2 - 1)/(2n^2 + 1)$ (ε and n are the dielectric constant and refraction index of the medium, respectively).[31]

[**] All lifetime measurements correspond to goodness-of-fit parameters $\chi^2 \geq 0.99$.

Table 2

Linear photophysical and photochemical parameters of **1** and **1**:Zn^{2+} complexes in organic (THF) and aqueous (water/ACN) medium: absorption λ_{abs}^{max} and fluorescence λ_{fl}^{max} maxima, Stokes shifts, maximum extinction coefficients ε^{max}, fluorescence quantum yields Φ, lifetimes τ and quantum yields of photochemical decomposition under one-photon irradiation Φ_{1PA}.

N/N	THF + Zn^{2+} ($M \approx 2.4 \cdot 10^{-4}$M)	Water/ACN (1:1)	Water/ACN (1:1) + Zn^{2+} ($M \approx 2.4 \cdot 10^{-4}$M)
λ_{abs}^{max}, nm	381 ± 1	380± 1	379± 1
λ_{fl}^{max}, nm	462 ± 1	534 ± 1	498 ± 1
Stokes shift, cm^{-1}	4600 ± 100	7590 ± 100	6300 ± 100
$\varepsilon^{max} \cdot 10^{-3}$, $M^{-1} \cdot cm^{-1}$	72 ± 5	49 ± 3	52 ± 3
Φ	0.73 ± 0.05	0.46 ± 0.03	0.51 ± 0.03
τ, ns*	1.18 ± 0.08	1.41 ± 0.08	1.27 ± 0.08
$\Phi_{1PA} \cdot 10^4$	3.0 ± 0.8	5.1 ± 2	6.0 ± 2

*All lifetime measurements correspond to goodness-of-fit parameters $\chi^2 \geq 0.99$.

Table 3

Calculated energies, *E*, oscillator strengths, *f*, and 2PA cross sections, δ_{2PA}, of the main electronic transitions for model compounds **1a**, **2a** and angles of space orientation, α, of the corresponding transition dipoles (relative to $S_0 \rightarrow S_1$).

N/N	1a			2a		
	$S_0 \rightarrow S_1$	$S_0 \rightarrow S_4$	$S_0 \rightarrow S_5$	$S_0 \rightarrow S_1$	$S_0 \rightarrow S_2$	$S_0 \rightarrow S_3$
E, eV (nm)	2.76 (449)	3.50 (354)	3.62 (343)	2.64 (469)	3.15 (394)	3.47 (357)
f	2.20	0.29	0.08	1.98	0.83	0.03
δ_{2PA}, GM	209	910	510	258	1306	567
α, degree	-	1.6	8.0	-	2.2	10.5

J Phys Chem B. Author manuscript; available in PMC 2011 July 22.